LAWRENCE
LIVERMORE
NATIONAL
LABORATORY

UCRL-JRNL-220096

Prediction and observation of tin and silver plasmas with index of refraction greater than one in the soft X-ray range

Jorge Filevich, Jonathan Grava, Mike Purvis, Mario. C. Marconi, Jorge. J. Rocca, Joseph Nilsen, James Dunn, Walter R. Johnson

March 24, 2006

Physical Review E

Prediction and observation of tin and silver plasmas with index of refraction greater than one in the soft X-ray range

Jorge Filevich[b], Jonathan Grava[a], Mike Purvis[a], Mario. C. Marconi[a], Jorge. J. Rocca[a,b]

NSF ERC for Extreme Ultraviolet Science and Technology

a. Department of Electrical and Computer Engineering

b. Department of Physics

Colorado State University, Fort Collins, CO 80523

Joseph Nilsen, James Dunn

Lawrence Livermore National Laboratory, Livermore, CA 94551

Walter R. Johnson

University of Notre Dame, Notre Dame, IN 46556

ABSTRACT

We present the calculated prediction and the experimental confirmation that doubly ionized Ag and Sn plasmas can have an index of refraction greater than one for soft x-ray wavelengths. Interferometry experiments conducted using a capillary discharge soft x-ray laser operating at a wavelength of 46.9 nm (26.44 eV) confirm that in few times ionized laser-created plasmas of these elements the anomalous dispersion from bound electrons can dominate the free electron contribution, making the index of refraction greater than one. The results confirm that bound electrons can strongly influence the index of refraction of numerous plasmas over a broad range of soft x-ray wavelengths confirming recent observations. The understanding of index of refraction at short wavelengths will become even more essential during the next decade as x-ray free electron lasers will become available to probe a wider variety of plasmas at higher densities and shorter wavelengths.

Keywords: X-ray laser, Interferometers; Index of refraction; Plasmas; Anomalous dispersion

1. INTRODUCTION

For many decades optical interferometers have been used to measure the electron density of plasmas using the assumption that the index of refraction of the plasma is due only to the free electrons [1-3], an assumption that implies that the index of refraction in the plasma should always be less than one. Over the last decade several interferometers [4-13] have been built to perform dense plasma diagnostics using probe wavelengths in the soft X-ray wavelength range of 14 to 72

nm (89 to 17 eV). Since the plasmas being studied were highly ionized, the analysis of the experiments done with these sources assumed that only the free electrons contribute significantly to the index of refraction.

Recent interferometry experiments of laser-produced Al plasmas conducted using probe wavelengths of 14.7 nm [12] and 13.9 nm [13] observed interference fringes that bent in the opposite direction than was expected, indicating that the index of refraction was greater than one. Analysis of the experiments showed that the anomalous dispersion from the resonance lines and absorption edges of the bound electrons have a larger contribution to the index of refraction with the opposite sign as that of the free electrons [12,14-16]. A significant result of the calculations is that the influence of the bound electrons on the index of refraction extends far from the absorption edges and resonance lines, affecting a broad range of wavelengths.

To understand how general this anomalous index of refraction effect is we have developed a new tool [17] that enables us to calculate the index of refraction for any plasma at any wavelength. This tool is a modified version of the INFERNO average atom code [18] that has been used for many years to calculate the absorption coefficients for plasmas at a given temperature and density. We have used the code to predict plasmas that will have an index of refraction greater than one at the 46.9 nm (26.44 eV) wavelength of the Ne-like Ar X-ray laser [19] developed at Colorado State University. This soft x-ray laser is a table-top capillary discharge laser that has been used for more than a decade as a research tool [20]. In this paper we present calculations of doubly ionized Ag and Sn plasmas that predict an index of refraction greater than one at this photon energy with experimental confirmation.

2. COMPUTATION OF THE INDEX OF REFRACTION AND ANALYSIS OF INTERFEROMETRY EXPERIMENTS

The traditional formula that assumes only free electron contribution to the index of refraction of a plasma is $n = (1 - N_{elec} / N_{crit})^{1/2}$ where N_{elec} is the electron density of the plasma and N_{crit} is the plasma critical density. At wavelength λ, $N_{crit} = \pi / (r_0 \lambda^2)$ where r_0 is the classical electron radius, 2.818×10^{-13} cm [3]. Since the density that can be probed is always less than the critical density (5.08×10^{23} cm^{-3} for the 46.9 nm Ne-like Ar X-ray laser) the index of refraction calculated this way would always be less than one. In typical experiments the electron density is much less than the critical density so the formula above can be approximated by $n = 1 - (N_{elec} / 2N_{crit})$. For a plasma of length L the number of fringe shifts observed in an interferometer equals

$$N_f = \frac{1}{\lambda}\int_0^L (1-n)dl$$

For the case of an uniform plasma the above formula simplifies to $N_f=(1 - n) L/\lambda$. Substituting the approximation described above for the index of refraction, the number of fringe shifts N_f equals $(N_{elec} L) / (2 \lambda N_{crit})$. The fringe shifts from the presence of a plasma are referenced against a set of reference fringes in the absence of any plasma. When analyzing an experiment one counts fringe shifts, that is how far the fringes have shifted compared to the reference fringes in terms of the fringe spacing, and converts the number of fringe shifts into electron density. Because the index of refraction is assumed always smaller than one, the fringes should shift in only one direction, determined by the geometry of the interferometer. From the anomalous results in the interferometry experiments [12,13,21] of the Al plasmas it is clear that these assumptions used to analyze the VUV

to soft x-ray interferometery are not always valid. Secondly, the bound electrons have a significant contribution to the index of refraction for the Al plasmas studied.

To determine the contribution of the bound electrons to the index of refraction one can make use of the relationship between the absorption coefficient and the index of refraction. The total absorption coefficient $\alpha = N_{ion}\sigma = 4\pi\beta / \lambda$ where N_{ion} is the ion density of the plasma, λ is the wavelength, σ is the absorption cross-section, β the imaginary part of the complex index of refraction n* defined by $n^* = 1 - \delta - i\beta$ where the real part of the index of refraction is $n = 1 - \delta$. The Henke tables [22] available from Lawrence Berkeley Laboratory tabulate the dimensionless optical constants f_1 and f_2 for neutral materials. These coefficients are related to δ and β by $\delta = f_1 N_{ion} / (2 N_{crit})$ and $\beta = f_2 N_{ion} / (2 N_{crit})$. Experimental data combined with theoretical simulations are used to obtain the total absorption cross-section σ from which we determine the optical constant $f_2 = \sigma / (2 \lambda r_0)$. We then derive the optical constant f_1 as a function of photon energy E using the Kramers-Kronig dispersion relation [23]. This involves taking the principal value of the integral

$$f_1(E) = Z_{nuc} + \frac{2}{\pi} P.V. \int_0^\infty \frac{f_2(\varepsilon)\varepsilon d\varepsilon}{E^2 - \varepsilon^2}$$

where Z_{nuc} is the atomic number of the element. In effect, all of the bound and free electrons are included when calculating the dispersion relation. For example, $Z_{nuc} = 50$ for a Sn plasma. For neutral materials the oscillator sum rules insure that f_1 goes to zero at zero energy and to Z_{nuc} at infinite energy. For an ionized plasma with average ionization Z* then $f_1 = Z^*$ at $E = 0$.

In the absence of any bound electrons f_1 is equivalent to the number of free electrons per ion. Taking the ratio of f_1 to the number of free electrons per ion gives the ratio of the measured electron density to the actual electron density. When the ratio is negative, the index of refraction is greater

than one, causing the fringes to bend in the direction opposite as expected in a free electron dominated plasma interferometry experiment.

To enable us to calculate the index of refraction for any plasma at any wavelength we used a modified version of the INFERNO average atom code. The INFERNO code [18] has been used for many years to calculate the ionization conditions and absorption spectrum of plasmas under a wide variety of conditions. This code uses the average-atom technique. For finite temperatures and densities, the INFERNO code calculates a statistical population for occupation of one-electron Dirac orbitals in the plasma. We use a non-relativistic version of INFERNO in this work to calculate bound and continuum orbitals and the corresponding self-consistent potential. By applying linear response theory we obtain an average-atom version of the Kubo-Greenwood equation [24,25] for the frequency-dependent conductivity of the plasma. The imaginary part of the complex dielectric function is proportional to the conductivity. The real part of the dielectric function can be found from its imaginary part using a Kramers-Kronig [23] dispersion relation. The details of the Kubo-Greenwood formula applied to the average-atom model are described in Ref. 17.

3. SEARCHING FOR ANOMALOUS DISPERSION AT 46.9 NM

To understand how general the bound electron contribution (anomalous dispersion) to the index of refraction is, we looked for materials that would have an index of refraction greater than one at 26.44 eV. As a first step in this search we looked at the Henke tables to find neutral materials that have an absorption edge near 26 eV. Sn (Z=50) immediately stood out as a candidate with the N_4 $4d_{3/2}$ and N_5 $4d_{5/2}$ edges at 24.9 and 23.9 eV. [22] The next step was to see if the f_1 coefficient is

negative at 26.44 eV. Finding negative f_1 values for neutral materials is usually a good clue to find negative f_1 in plasmas that are only a few times ionized. However the lowest published value for f_1 in the Henke tables is at an energy of 30 eV. Since the absorption coefficient f_2 has published values down to 10 eV we use the Kramers-Kronig dispersion relation to calculate our own estimate of f_1 below 30 eV, making sure we adjusted f_1 by a constant value to agree with the published Henke data above 30 eV. We looked at Sn and other nearby materials with Z = 42 to 51. Figure 1 shows our estimate of f_1 for various materials. Mo, Pd, and Sb, have positive f_1 at 26.44 eV even though Mo and Pd have negative values at other energies while Sb stays positive for the energies shown in the figure. Ag and Sn both have negative values of f_1 near 26 eV. Ag has negative values over the entire range from 10 to 35 eV while Sn is negative from 21 to 60 eV. For Sn we estimate that f_1 is -1.8 while for Ag we estimate that f_1 is –2.1 at 26.44 eV. Both Ag and Sn look to be promising candidates to do further calculations. Since the reflectivity of materials at grazing incidence depends on f_1 being positive, an interesting experiment to verify the negative f_1 values would be to check whether the X-ray laser reflects off the material at grazing incidence as proposed by Smith and Barkyoumb [26].

4. MODELING OF TIN AND SILVER PLASMAS

For neutral materials like Sn the absorption coefficient at the 46.9 nm wavelength corresponding to the Ne-like Ar laser would be too high to observe fringes in an interferometer but we know that the absorption edge moves to higher energy when the material is ionized. From the Dirac-Slater calculations of Scofield [27] the ionization potential of the outer electron for singly ionized Sn is 12.9 eV and doubly ionized is 30.1 eV. Doubly ionized Sn look promising for this work since the

26.44 eV X-ray laser would not have enough energy to photo-ionize Sn^{2+} and therefore the absorption coefficient will be much smaller than for neutral Sn. From Ref. 28 we see that Sn^{2+} has 3 absorption lines at 26.72, 27.58, and 28.03 eV that have been measured experimentally. These are the $4d^{10}5s^2\ ^1S_0$ - $4d^9 5s^2 5p^1\ ^3P_1$, $^1P_1$, $^3D_1$ lines with absorption oscillator strengths of 0.071, 0.801, 0.067 respectively. The 26.44 eV Ne-like soft x-ray laser is situated on the low energy side of these strong lines, so these lines will have a negative contribution to the f_1 value at this energy.

Looking at Sn^{2+}, we estimated the absorption coefficient f_2 by using the neutral absorption coefficient published in the Henke tables for energies above the calculated photo-ionization edge at 30 eV. We combined this with our multi-configuration Dirac-Fock (MCDF) calculations [29] for the low energy 5s – 5p lines near 5 and 10 eV, and the measured 4d – 5p lines near 27 eV [28]. Using this absorption coefficient in the Kramers-Kronig dispersion relation we then determined the optical constant f_1 versus photon energy, as shown by the dotted line in Fig. 2. At the 26.44 eV energy of the Ne-like Ar soft x-ray laser line we estimate that f_1 is -13, which makes the index of refraction larger than one. The most important contribution to f_1 at this energy is from the measured 4d – 5p lines at 26.72, 27.58, and 28.03 eV [28]. If only the free electrons contributed to the index then f_1 would be 2. This suggests that experiments with Sn^{2+} plasmas will observe interference fringes bending 6.5 times more than expected for the actual plasma density and the interference fringes would bend in the opposite direction due to the index of refraction being larger than one.

A second method to estimate the index of refraction for the Sn plasma is to use the average atom code. We choose a Sn plasma with an ion density of 10^{20} cm^{-3} to model. By varying the temperature of the plasma we can find the conditions where the Sn plasma would be approximately doubly-ionized. At temperatures of 3, 4, 5, and 10 eV we calculate the mean ionization, Z*, to be 1.49, 1.98, 2.40, and 4.25, respectively. Since Z* = 2 is doubly-ionized on average we chose a temperature of 4

eV to study. The solid line in Fig. 2 shows the optical constant f_1 versus photon energy calculated by the average atom code. This is compared with the calculation of f_1 for Sn^{2+} described above, shown by the dotted line. We have excellent agreement between the two calculations in the region near 26 eV. At 26.44 eV the average atom code predicts $f_1 = -10$. It is somewhat fortuitous that average atom calculations have the strong 4d-5p absorption line within 0.1 eV of the experimentally measured values since normally we would have to shift the average atom results slightly to line up the relevant absorption features [15,16]. This underscores the importance of having spectroscopic experimental data together with the calculations to predict f_1.

There is insufficient experimental data to estimate the f_1 value for Ag plasmas as described above for Sn but based on calculations doubly-ionized Ag will be expected to have 4d – 4f and 4d – 6p lines in the 25 to 30 eV region that could result in a negative f_1 value at 26.44 eV. In addition the photo-ionization absorption edge for doubly-ionized Ag is at 35 eV, which means absorption in the Ag^{2+} plasma, should be small for the Ne-like Ar 26.44 eV laser line allowing interferometry experiments. Average atom calculations of Ag plasmas with ion density of 10^{20} cm^{-3} and a temperature of 4 eV were performed. Under these conditions $Z^* = 2.08$ indicates a doubly-ionized plasma and Fig. 3 shows the predicted optical constant f_1 versus photon energy. The structure is more complicated than for Sn because of multiple strong lines but the average atom code predicts f_1 is -7 at 26.44 eV. It also predicts that f_1 will be less than zero from 21.8 to 27.8 eV and 28.1 to 38.6 eV. However, there is substantial variation in the magnitude of f_1 over this range. In the absence of experimental data on the positions of the absorption lines we are less confident in the absolute position of the energy scale but certainly expect experiments to show anomalous dispersion in this photon energy range.

5. INTERFEROMETER EXPERIMENTS WITH TIN AND SILVER PLASMAS

The experiments were conducted combining a 46.9 nm table-top Ne-like Ar capillary discharge laser [30] with an amplitude division Diffraction Grating Interferometer (DGI) [6,31]. The experimental set up is schematically illustrated in Fig. 4. The DGI is set in a skewed Mach-Zehnder configuration using diffraction gratings as beam splitters. The light incident on the first grating is diffracted in the zero and first orders with approximately equal intensity by selecting the blaze angle on the gratings. The beams that form the two arms of the interferometer are reflected at a grazing incidence angle toward a second diffraction grating using two 35 cm long gold-coated mirrors. The second diffraction grating recombines the two beams such that they exit the interferometer propagating with a small angular difference, selected to produce fringes of the spacing required by the experiment. The Sn or Ag plasmas were created by illuminating a target with a pulsed laser beam. The target was placed intersecting the zero order path of the interferometer at a location between the long mirror and the second diffraction grating. The plasma with corresponding fringe pattern was imaged with ~25× magnification using Sc/Si multilayer optics [32] onto a Microchannel plate charge-coupled device (MCP-CCD) detector combination.

The compact 46.9 nm Ne-like Ar capillary discharge-pumped laser generated laser pulses of ~1 ns duration and energies of ~0.1 mJ. The high brightness of this source helps overcome the self-emission coming from the laser-created plasma. The good beam spatial coherence [33] produces high quality interferograms with high fringe visibility when combined with the DGI. The soft x-ray laser was laser triggered achieving a measured jitter of ~1-2 ns. The interferometer and the

alignment procedure are described in more detail in previous publication [31].

The plasma was generated by irradiating a 1 mm long semi-cylindrical target with an 800 nm wavelength laser pulse of 120 ps (FWHM) and up to 1 J of energy. A line focus ~1.7 mm long and 310 μm wide, resulting in an irradiance of ~1.3×10^{12} W cm^{-2} was formed in the target plane using the combination of a 7 m focal length spherical lens and a variable cylindrical lens created by combining a positive and a negative 1 m focal length cylindrical lenses. The line focus shape and the intensity of the heating beam in the target plane were monitored on every shot by imaging the reflection off a 4 % beam splitter onto a CCD camera. The targets consisted of semi-cylindrical cavities 500 μm in diameter machined on the front surface of 99.9 % pure slabs of Sn and Ag, 1 mm × 4 mm × 4 cm in size, as shown in the detail in Fig 4. This target geometry combined with a relatively wide line focus irradiation generates a hot dense plasma on the axis of the cavity. The plasma remains sufficiently dense to allow for the observation of fringe shifts as the plasma recombines into ions with low charge states following expansion and cooling.

Figures 5 and 6 show interferograms corresponding to two different times during the evolution of Tin and Silver plasmas, respectively. At 4.5 ns after the arrival of the heating laser the creation of a concentrated region of dense plasma is observed near the geometrical center of the groove. This dense plasma region is formed by the convergence of the plasma from the target wall. At this early time in the evolution, the plasma is hot and highly ionized, and the contribution of bound electrons to the index of refraction (and therefore to the fringe shifts) can be neglected. The dominant contribution of the free electrons to the index of refraction causes the interference fringe to bend to the right. With the assumption of negligible bound electron contribution it is possible to compute electron density maps of the plasmas, resulting in a peak density of 2×10^{19} cm^{-3} for the case of the Sn plasma.

While not shown in the figures, later in time, starting about 20 ns after plasma irradiation, the plasma becomes very absorbent as it cools down near the target surface and further out the interference fringes are flattened, an indication that the index of refraction is now close to 1. Such fringe behavior indicates that either the plasma density has decreased to very low values, or that the bound electrons contribute significantly to the index of refraction and compensate for the contribution of free electrons resulting in an index of refraction close to one. As discussed below interferograms obtained at even later times confirm the latter is the dominant cause.

The images acquired at time delay of 33 ns for Tin, Fig. 5 (b), and 35 ns for Silver, Fig. 6 (b), show even higher absorption, now extending to the region where the plasma had collided. At this time the interference fringes are observed to bend toward the target, indicating an index of refraction greater than one. The black vertical lines drawn on the late images of Fig. 5 and 6 represent the position of a reference fringe in the absence of plasma, indicating that the fringes are shifting in the opposite direction as expected if only free electrons where contributing to the index of refraction. A naive interpretation of the results would yield an unphysical negative electron density.

6. CONCLUSIONS

The index of refraction is an essential plasma property used to compute the transport of radiation, understand the deposition of laser energy in the plasmas, and measure key plasma parameters such as electron density. For decades the analysis of the plasma diagnostics, such as interferometry, have relied on the approximation that the index of refraction in plasmas is due solely to the free electrons. This general assumption makes the index of refraction less than one. Recent

soft x-ray laser interferometry experiments with Al plasmas at wavelengths of 14.7 nm and 13.9 nm have shown that this approximation is not always valid [11,12]. Analysis of the data demonstrated that bound electrons can contribute significantly to the index of refraction of multiply ionized plasmas at soft X-ray wavelengths in the vicinity of absorption lines and edges.

The results of the present study, which involved a significantly different soft x-ray wavelength, 46.9 nm, and plasmas of two different elements, Sn and Ag, show that index of refraction greater than one are a frequently encountered phenomena in multiply ionized plasmas. This finding has broad practical significance, and affecting for example the analysis of soft x-ray laser interferometry measurements of plasmas. While soft X-ray laser interferometry allows measurements of higher plasma densities because of better spatial resolution, reduced absorption and reduced deflection angles, neglecting the contribution of bound electrons to the index of refraction could, in some cases, constitute a significant systematic error in the determination of the electron density. It is important to note that the importance of the bound electron contribution is not limited to plasmas with a low mean ion charge. Nevertheless, most hot plasmas that are many times ionized can be confidently probed using soft X-ray laser interferometry, and it is possible to select the probe wavelengths to avoid the contribution from bound electrons to the index in the particular plasma of interest. This shows the need to do some theoretical modeling of the plasma to verify that experiments are being done in a regime where the free electron approximation for the index of refraction is valid. As X-ray free electron lasers and other sources become available [34] during the next decade to probe a wider variety of plasmas at higher densities the contribution of bound electrons to the index of refraction will have to be taken into account.

ACKNOWLEDGEMENTS

This research was sponsored by the National Nuclear Security Administration under the Stewardship Science Academic Alliances program through U. S. Department of Energy Research Grant #---, with the work of LLNL researchers supported under the auspices of the U. S. Department of Energy by the University of California Lawrence Livermore National Laboratory under contract No.W-7405-ENG-48. One author (WRJ) was supported in part by NSF Grant No. PHY-0139928. The work made use of the facilities of the NSF ERC Center for Extreme Ultraviolet Science and Technology, NSF award EEC-0310717.

REFERENCES

[1] D.T. Attwood, D.W. Sweeney, J.M. Auerbach and P.H.Y. Lee, Phys. Rev. Lett. **40**, 184, (1978).

[2] G. J. Tallents, J. Phys. D. **17**, 721 (1984).

[3] H. R. Griem, *Principles of Plasma Spectroscopy*, (Cambridge University Press, Cambridge, 1997) p. 9

[4] L. B. Da Silva, T. W. Barbee, Jr., R. Cauble, P. Celliers, D. Ciarlo, S. Libby, R. A. London, D. Matthews, S. Mrowka, J. C. Moreno, D. Ress, J. E. Trebes, A. S. Wan, and F. Weber, Phys. Rev. Lett. **74**, 3991 (1995).

[5] J.J. Rocca, C.H. Moreno, M.C. Marconi and K. Kanizay, Optics Letters **24**, 420, (1999).

[6] J. Filevich, K. Kanizay, M.C. Marconi, J.L.A. Chilla, and J.J. Rocca, Optics Letters 25, 356, (2000).

[7] R.F. Smith, J.Dunn, J. Nilsen, V.N. Shlyaptsev, S. Moon, J. Filevich, J.J. Rocca, M.C. Marconi, J.R. Hunter, and T.W. Barbee, Jr., Physical Review Letters **89**, 065004, (2002).

[8] J.J. Rocca, E.C. Hammarsten, E. Jankowska, J. Filevich, M.C. Marconi, S. Moon, and V.N. Shlyaptsev, Physics of Plasma **10**, 2031, (2003)

[9] J. Filevich, J.J. Rocca, E. Jankowska, E.C. Hammarsten, M.C. Marconi, S.Moon and V.N. Shlyaptsev, Physical Review E **67**, (2003).

[10] Albert F., Joyeux D., Jaegle P., Carillon A., Chauvineau J.P., Jamelot G., Klisnick A., Lagron J.C., Phalippou D., Ros D., Sebban S., Zeitoun P. Optics Communications, Volume 142, Number 4, 15 October 1997, pp. 184-188(5)

[11] D. Descamps, C. Lyngå, J. Norin, A. L'Hullier, C.-G. Wahlström, J.-F. Hergott, H. Merdji, P. Salières, M. Bellini, and T. W. Hänsch, Opt. Lett. **25**, 135 (2000).

[12] J. Filevich, J. J. Rocca, M. C. Marconi, S. Moon, J. Nilsen, J. H. Scofield, J. Dunn, R. F. Smith, R. Keenan, J. R. Hunter, and V. N. Shlyaptsev, Phys. Rev. Lett. **94**, 035005 (2005).

[13] H. Tang, O. Guilbaud, G. Jamelot, D. Ros, A. Klisnick, D. Joyeux, D. Phalippou, M. Kado, M. Nishikino, M. Kishimoto, K. Sukegawa, M. Ishino, K. Nagashima, and H. Daido, Appl. Phys. B **78**, 975 (2004).

[14] J. Nilsen and J. H. Scofield, Opt. Lett. **29**, 2677 (2004).

[15] J. Nilsen and W. R. Johnson, Applied Optics **44**, 7295 – 7301 (2005).

[16] J. Nilsen, W. R. Johnson, C. A. Iglesias, and J. H. Scofield, J. Quant. Spectrosc. Radiat. Transfer **99**, 425 – 438 (2006).

[17] W. R. Johnson, C. Guet, and G. F. Bertsch, J. Quant. Spectrosc. Radiat. Transfer **99**, 327 – 340 (2006).

[18] D. A. Liberman, JQSRT **27**, 335 (1982).

[19] J. J. Rocca, V. Shlyaptsev, F. G. Tomasel, O. D. Cortázar, D. Hartshorn, and J. L. A. Chilla, Phys. Rev. Lett. **73**, 2192–2195 (1994).

[20] J.J. Rocca, M. Frati, B. Benware, M. Seminario, J. Filevich, M.C. Marconi, K. Kanizay, A. Ozols, I.A. Artiukov, A. Vinogradov, Y.A. Uspenskii, Comptes Rendus De L' Academie Des Sciences Serie IV, Physique Astrophysique **8**, 1065, (2000)

[21] J. Filevich, J. J. Rocca, M. C. Marconi, S. Moon, J. Nilsen, J. H. Scofield, J. Dunn, R. F. Smith, R. Keenan, J. R. Hunter, and V. N. Shlyaptsev, J. Quant. Spectrosc. Radiat. Transfer **99**, 165 – 174 (2006).

[22] B. L. Henke, E. M. Gullikson, and J. C. Davis, At. Data Nucl. Data Tabl. **54**, 181 - 342 (1993).

[23] L. D. Landau and E. M. Lifshitz, *Electrodynamics of Continuous Media*, (Pergamon, New York, 1984) pp. 280 – 283

[24] D. A. Greenwood, Proc. Phys. Soc. London **715**, 585 (1958).

[25] R. Kubo, J. Phys. Soc. Jpn. **12**, 570 (1957).

[26] D.Y. Smith and J.H. Barkyoumb, Physical Review B. 6, **41**, 11529 (1990)

[27] James Scofield, private communication.

[28] P. Dunne, F. O'Reilly, G. O'Sullivan, and N. Murphy, J. Phys. B **32**, L597 (1999).

[29] I. P. Grant, B. J. McKenzie, P. H. Norrington, D. F. Mayers, and N. C. Pyper, Comput. Phys. Commun. **21**, 207 (1980).

[30] B. R. Benware, C. D. Macchietto, C. H. Moreno, and J. J. Rocca, Phys. Rev. Lett. 81, 5804–5807 (1998)

[31] J. Filevich, J. J. Rocca, M. C. Marconi, R. F. Smith, J. Dunn, R. Keenan, J. R. Hunter, S. J. Moon, J. Nilsen, A. Ng, and V. N. Shlyaptsev, Appl. Opt. 43, 3938-3946 (2004)

[32] Y. A. Uspenskii, V. E. Levashov, A. V. Vinogradov, A. I. Fedorenko, V. V. Kondratenko, Y. P. Pershin, E. N. Zubarev, and V. Y. Fedotov, Opt. Lett. **23**, 771-773 (1998)

[33] Y. Liu, M. Seminario, F. G. Tomasel, C. Chang, J. J. Rocca and D. T. Attwood, Phys. Rev. A **63**, 033802, (2001)

[34] A. Meseck, M. Abo-Bakr, D. Krämer, B. Kuske, and S. Reiche, Nucl. Inst. And Meth. A **528**, 577 (2004).

Figure Captions:

Fig. 1 Optical constant f_1 versus photon energy for various neutral materials. These values are an extrapolation of the Henke tables to lower energy.

Fig. 2. Optical constant f_1 versus photon energy calculated directly for Sn^{2+} (dotted line) and by the average atom code (solid line) for a Sn plasma with an ion density of 10^{20} cm^{-3}, a temperature of 4 eV, and Z* = 1.98.

Fig. 3. Optical constant f_1 versus photon energy calculated by the average atom code for a Ag plasma with an ion density of 10^{20} cm^{-3}, a temperature of 4 eV, and Z* = 2.08.

Fig. 4. Experimental setup showing the Diffraction Grating Interferometer and detailed schematic of the 500 μm x 1000 μm semi-cylindrical targets used.

Fig. 5. Soft x-ray interferograms corresponding to two times during the evolution of Sn plasmas generated by illuminating a 500 μm diameter Sn semi-cylindrical groove with a ~1.3×10^{12} W cm^{-2} 800 nm, 120 ps laser beam. The early shot (4.5 ns from the heating beam) shows a plasma for which the fringes shift to the right, while the later frame (33 ns) shows fringes that bend to the left of the reference line (drawn), an indication of an index of refraction greater than one.

Fig. 6. Soft x-ray interferometry data similar to that in figure 5, but for the case of an Ag plasma.

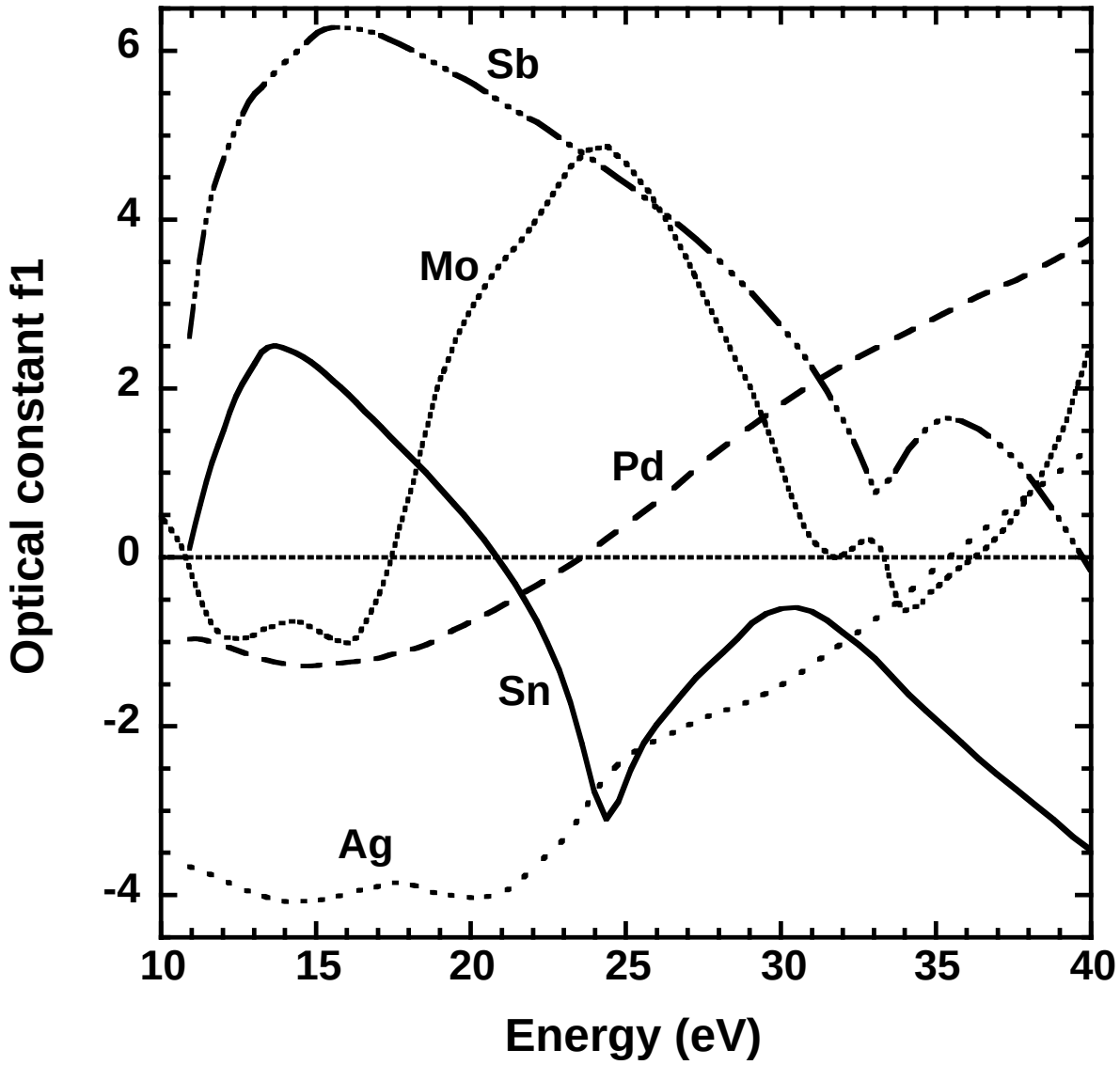
Optical constant f1
Energy (eV)
Sb
Mo
Pd
Sn
Ag
6
4
2
0
-2
-4
10
15
20
25
30
35
40

Figure 1

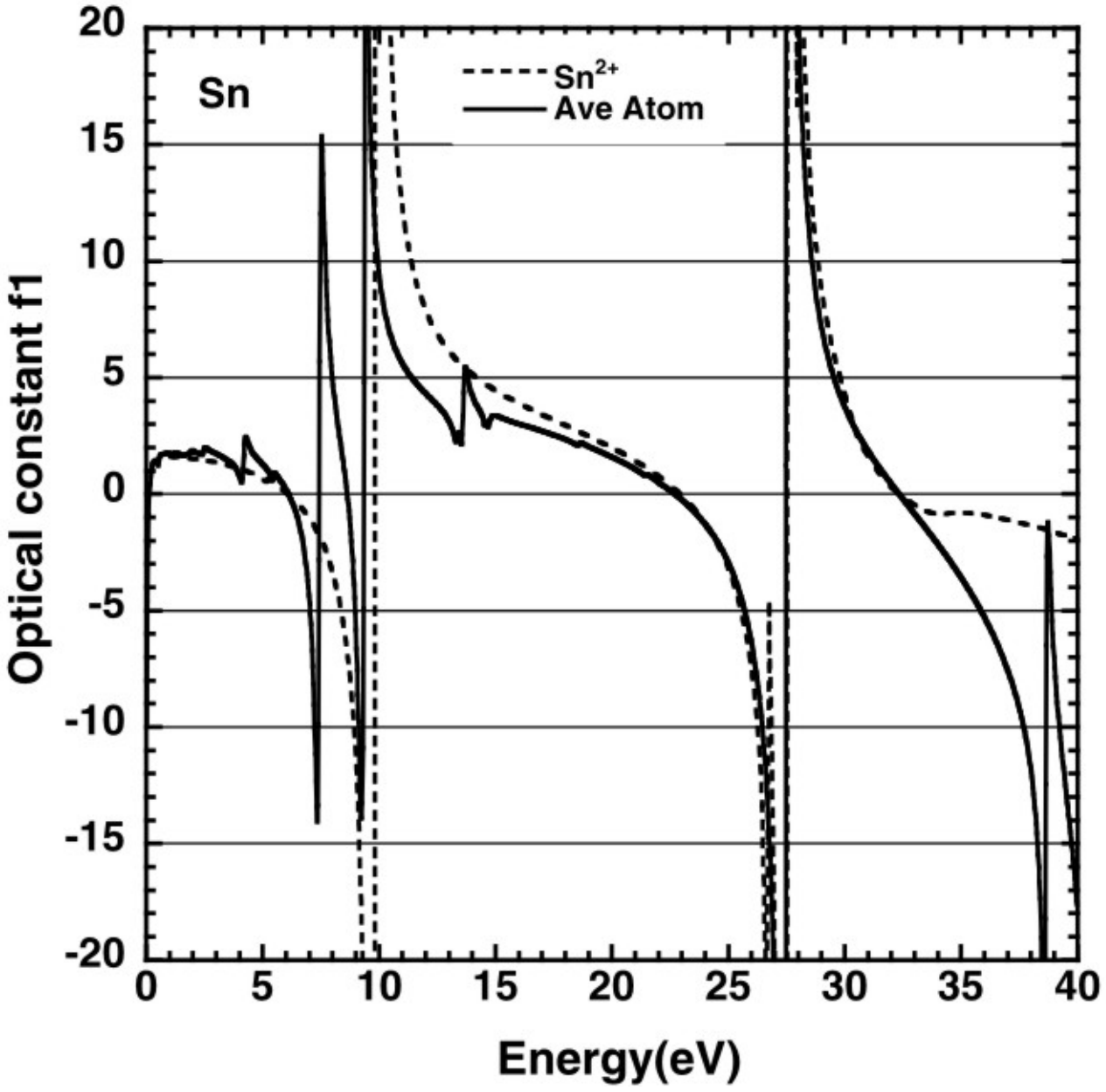
Sn
Sn2+
Ave Atom
Optical constant f1
Energy(eV)
20
15
10
5
0
-5
-10
-15
-20
0
5
10
15
20
25
30
35
40

Figure 2

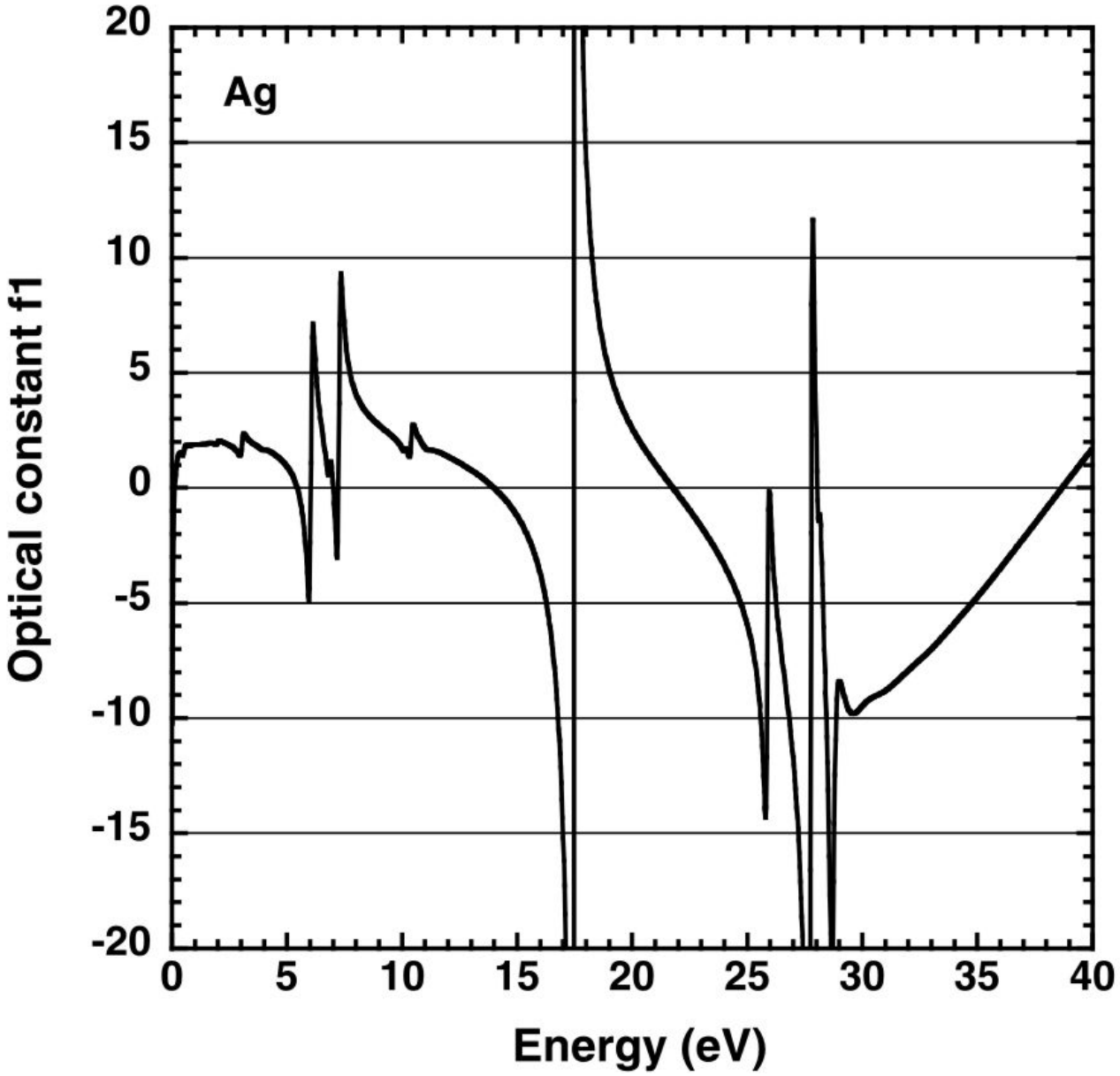
Ag
Optical constant f1
Energy (eV)
20
15
10
5
0
-5
-10
-15
-20
0
5
10
15
20
25
30
35
40

Figure 3

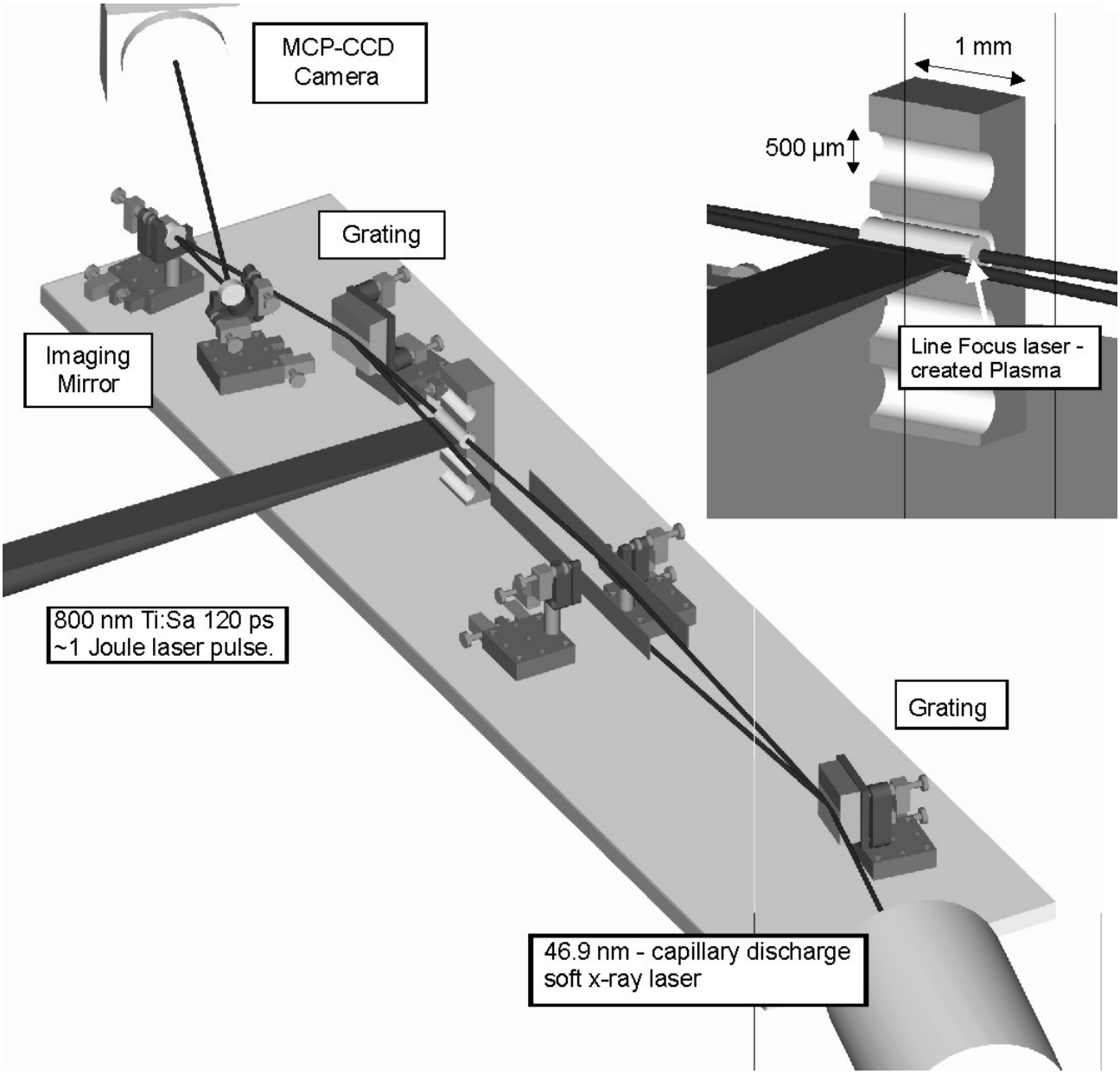
MCP-CCD
Camera
1 mm
500 µm
Grating
Imaging
Mirror
Line Focus laser -
created Plasma
800 nm Ti:Sa 120 ps
~1 Joule laser pulse.
Grating
46.9 nm - capillary discharge
soft x-ray laser

Figure 4

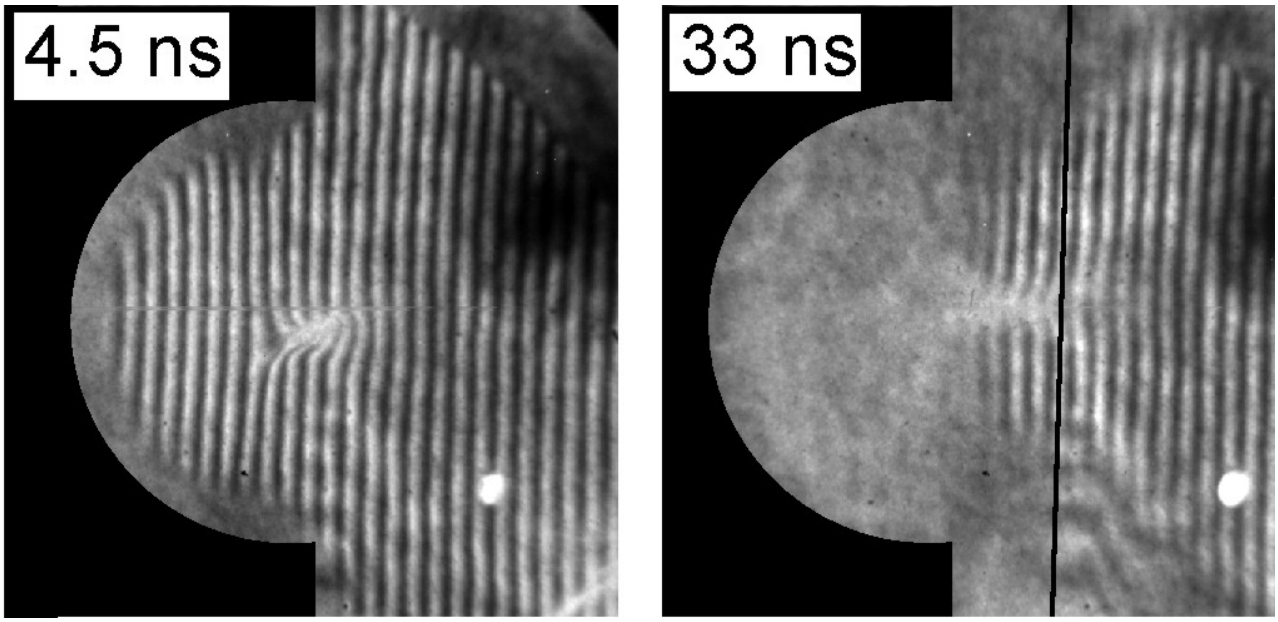

Figure 5

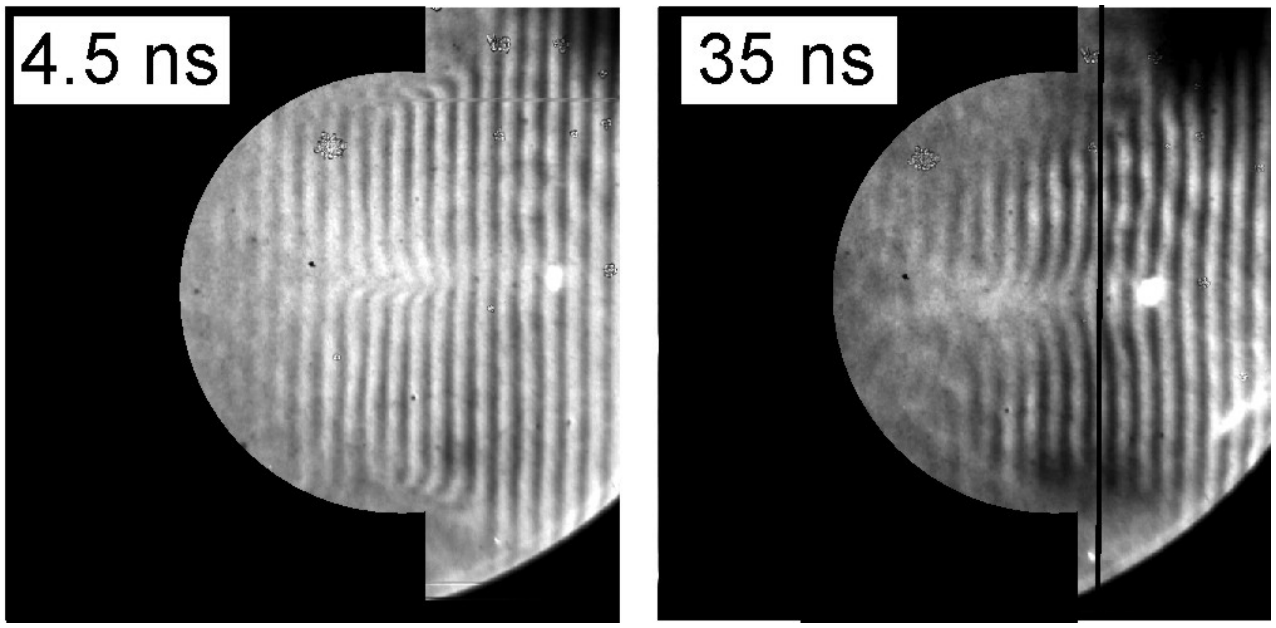

Figure 6